

Acoustical modeling of the saxophone mouthpiece as a transfer matrix^{a)}

Song Wang,^{b)} Esteban Maestre,^{c)} and Gary Scavone

Computational Acoustic Modeling Laboratory, Center for Interdisciplinary Research in Music Media and Technology, Schulich School of Music, McGill University, Montreal, Quebec H3A 1E3, Canada

ABSTRACT:

This paper proposes an acoustic model of the saxophone mouthpiece as a transfer matrix (TM). The acoustical influence of the mouthpiece is investigated, and the TM mouthpiece model is compared to previously reported mouthpiece representations, including cylindrical and lumped models. A finite element mouthpiece model is first developed, from which the TM model is derived, and both models are validated by input impedance measurements. The comparison of acoustic properties among different mouthpiece models shows that the TM mouthpiece is more accurate than the other two models, especially in preserving the high-frequency acoustic characteristics. The TM model also produces the best overall tuning of the first several impedance peaks when coupled to a measured saxophone impedance. The internal and radiated sound pressure are synthesized for an alto saxophone connected to different mouthpiece models by jointly modeling the input impedance and the radiation transfer function using recursive parallel filters. Differences are found among mouthpiece models in terms of oscillation thresholds, playing frequencies, spectral centroids, pressure waveforms, and bifurcation delays, which can be partially explained by differences in the tuning and high-frequency characteristics. © 2021 Acoustical Society of America. <https://doi.org/10.1121/10.0003814>

(Received 4 November 2020; revised 24 February 2021; accepted 25 February 2021; published online 18 March 2021)

[Editor: Nicholas J. Giordano]

Pages: 1901–1912

I. INTRODUCTION

The mouthpiece of the saxophone, like that of the clarinet, is a fundamental component of the instrument, onto which a reed is attached and through which a player can excite the instrument. There are many different makes and models of mouthpieces available, and variations of geometry of the mouthpiece can have important influence on the sound and playability of the instrument (Pipes, 2018; Wyman, 1972). The ways in which the mouthpiece exerts this influence can be associated with the underlying solid, fluid, and acoustic fields and their interactions. For example, the tip opening height and the curvature of the lay are critical aspects of the reed-mouthpiece interaction (Avanzini and van Walstijn, 2004), different reed channel lengths alter the flow profile (van Zon *et al.*, 1990), and the chamber geometry of the mouthpiece impacts the acoustic input impedance (Andrieux *et al.*, 2016). Moreover, the interactions among different fields, like the fluid-structure interactions (da Silva, 2008) and the aeroacoustics (Hirschberg *et al.*, 1996), also play an important role. In this paper, we focus on the acoustical modeling of the mouthpiece, with the goal of achieving a more accurate and flexible representation of an actual saxophone mouthpiece that can be applied both to sound synthesis and to investigate mouthpiece design variations. This model is also compared to previously reported mouthpiece acoustic representations.

The saxophone body is a truncated conical air column with modal frequencies that are not harmonically related (Ayers *et al.*, 1985). The mouthpiece completes the conical frustum by providing the volume equivalent to that of the missing part of the cone so that the fundamental frequency and the harmonics are better tuned (Benade, 1990). For the low-frequency range, where the wavelength is large compared to the dimension of the mouthpiece, the mouthpiece can be modeled as a parallel acoustic compliance that is determined only by the volume of the mouthpiece (Chen *et al.*, 2009; Kergomard *et al.*, 2016). However, such a lumped model is less accurate at high frequencies, where the admittance of the parallel acoustic compliance overwhelms that of the resonator. The “cyclone” model provides another way to represent the mouthpiece as a pure cylinder (Scavone, 2002). Similar to the lumped mouthpiece model, the volume of the cylinder is the same as that of the missing part of the cone. The cylindrical mouthpiece is coupled to the saxophone body based on mass conservation and pressure continuity at the junction between the cylinder and the conical frustum. Kergomard *et al.* (2016) extended the cylindrical mouthpiece model by allowing a cross section discontinuity. It is shown that the behavior of the cylindrical mouthpiece model, including the resulting mouthpiece internal pressure waveform and the inharmonicity of the complete instrument, highly depends on the mouthpiece length and diameter. While the cylindrical model with a short length resembles the lumped model, more and more higher-frequency components are introduced as the mouthpiece becomes longer. The dependence of the acoustic behavior on the variable length of the cylindrical mouthpiece model

^{a)}This paper is part of a special issue on Modeling of Musical Instruments.

^{b)}Electronic mail: song.wang5@mail.mcgill.ca, ORCID: 0000-0002-3012-5715.

^{c)}ORCID: 0000-0002-0712-639X.

might bring about uncertainties when used in a sound synthesis scheme. A cylinder-cone mouthpiece model was proposed by van Walstijn and Campbell (2003) for the clarinet. It approximates the mouthpiece as a cylindrical section followed by a conical section. However, the structure near the tip of a real mouthpiece is more like a cone, and the remaining part of the mouthpiece is more cylindrical so that the neck of the saxophone can be easily attached. Considering the mouthpiece is a non-reciprocal acoustic unit, reversing the order of the cone and the cylinder can lead to a very different behavior. A more precise model of the saxophone mouthpiece was proposed (Andrieux *et al.*, 2014; Andrieux *et al.*, 2016) using the finite element (FE) method. The FE model was validated by the measured mouthpiece input impedance and was coupled to a measured input impedance of the saxophone body to study the mouthpiece geometry's influence on the instrument. To the authors' knowledge, this is the only work that has considered a more accurate geometry of a mouthpiece. However, the FE model is time-consuming to develop and compute, making it inappropriate for sound synthesis and the analysis of transient behaviors.

To overcome the limitations of the above-mentioned models, we propose to model the mouthpiece as a transfer matrix (TM). The TM model is derived from the FE model so that the acoustic properties contributed by the complex mouthpiece geometry are intrinsically retained. For this reason, the TM mouthpiece model is more accurate than the cylindrical and lumped mouthpiece models, as shown by comparing the measured input impedance of a system composed of a mouthpiece coupled to a truncated cone (the mouthpiece-cone system) with that calculated using different mouthpiece models. As well, the TM model provides a compact mouthpiece representation that can be used for real-time sound synthesis. In this paper, the sound of the saxophone with different mouthpiece models is synthesized using the framework proposed by (Maestre and Scavone, 2016; Maestre *et al.*, 2018). The differences in the sound, as well as the dynamics, among different mouthpiece models are explored and discussed.

The paper is organized as follows: Sec. II describes the FE model and the derivation of the TM model. The validations of the FE model and the TM model, as well as the details of the input impedance measurement, are presented in Sec. III. The comparison of acoustic properties between the TM mouthpiece and other mouthpiece representations is shown in Sec. IV. The synthesis model is reviewed in Sec. V, and the comparisons of the sound and the dynamics behavior are presented and discussed. Finally, the perspectives of this study are discussed in Sec. VI.

II. ACOUSTICAL MODELING OF THE SAXOPHONE MOUTHPIECE

A. Finite element modeling of the mouthpiece

A three-dimensional (3D) alto saxophone mouthpiece model was built using the computer-aided design (CAD) software Autodesk[®] Fusion 360. The reed was assumed to be fixed in an open position but with closed side slits, resulting in a rectangular tip window at the input end. The extracted inner geometry is shown in Fig. 1(a).

The 3D model was imported into COMSOL Multiphysics[®] for the FE simulation. A plane wave pressure source was set as the inlet boundary condition at the tip window of the mouthpiece. Viscothermal losses at the wall surfaces were imposed using an acoustic admittance defined as (Chaigne and Kergomard, 2016)

$$Y_{wall} = \frac{1}{\rho c} \sqrt{jk} \left[\sin^2 \theta \sqrt{l_v} + (\gamma - 1) \sqrt{l_t} \right], \quad (1)$$

with ρ the fluid density, c the speed of the sound, k the wavenumber, θ the angle of the incidence of the wave, $l_v = \mu/\rho c$ the vortical characteristic length, $l_t = l_v/Pr$ the thermal characteristic length, γ the ratio of specific heats, μ the fluid dynamic viscosity, and Pr the Prandtl number. The mesh of the FE model, shown in Fig. 1(b), was constructed with a maximum element size of 6 mm, which allows the model to have at least 7–8 nodes per wavelength at 8 kHz.

B. TM modeling of the mouthpiece

The TM method has been widely applied to the study of the wind instrument resonator, including the effects of the tone hole (Keefe, 1990; Lefebvre, 2010) and the cutoff frequency (Petersen *et al.*, 2019), to name a few. It is based on the acoustical two-port theory that assumes a linear acoustical system with two terminals (Pierce, 2019). The black-box region between terminals can be characterized by a 2×2 matrix written as

$$\mathbf{T} = \begin{bmatrix} T_{11} & T_{12} \\ T_{21} & T_{22} \end{bmatrix}, \quad (2)$$

with all the matrix elements as functions of frequency. It defines the relationship of the acoustic pressure and volume velocity between the input and the output of the acoustic system:

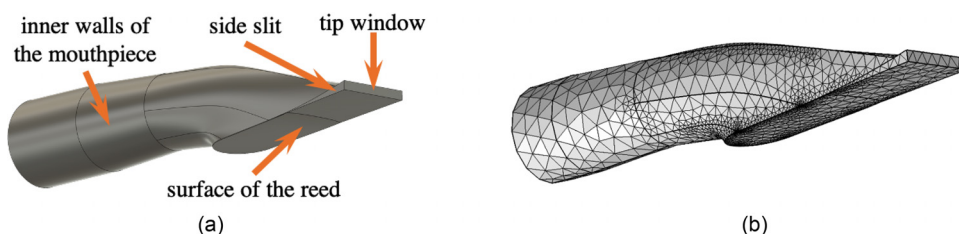


FIG. 1. (Color online) The (a) inner geometry and the (b) meshing of the mouthpiece.

$$\begin{bmatrix} P_o \\ Z_o^c U_o \end{bmatrix} = \mathbf{T} \begin{bmatrix} P_i \\ Z_i^c U_i \end{bmatrix}, \quad (3)$$

where $Z_c = \rho c/S$ is the characteristic acoustic impedance and S is the cross section area. The subscripts i and o represent the input and the output side of the acoustic system, respectively.

The TM of the mouthpiece is built based on several assumptions. First of all, the acoustic system has to be linear and passive. This is true only when the sound source of the saxophone is decoupled from the mouthpiece. Even though the reed is treated as part of the boundaries in the mouthpiece, its vibration is not. In this way, the excitation and the nonlinearity of the system can be modeled separately, and the mouthpiece can be treated as a linear and passive acoustic system. Another assumption is that only the propagating mode is considered on both the input and the output surface. This assumption is satisfied at the input surface by assuming a plane wave sound source, as it was set in the FE model. On the output side, it is assumed that the discontinuity between the mouthpiece and the connected resonator, e.g., a saxophone bore or a truncated cone, is small enough that any excited evanescent modes decay sufficiently within the mouthpiece and do not interact with other discontinuities. In addition, it is also assumed that the discontinuities within the mouthpiece are far enough from the output plane.

To derive the TM of the mouthpiece, the two-load method was used by running the FE simulation twice with two different output boundary conditions (Lefebvre, 2010). With the simulated pressure and volume velocity at both the input and the output, the following linear equation system can be solved to obtain the four elements of the TM:

$$\begin{bmatrix} p_o^1 & Z_o^c U_o^1 & 0 & 0 \\ 0 & 0 & p_o^1 & Z_o^c U_o^1 \\ p_o^2 & Z_o^c U_o^2 & 0 & 0 \\ 0 & 0 & p_o^2 & Z_o^c U_o^2 \end{bmatrix} \begin{bmatrix} T_{11} \\ T_{12} \\ T_{21} \\ T_{22} \end{bmatrix} = \begin{bmatrix} p_i^1 \\ Z_i^c U_i^1 \\ p_i^2 \\ Z_i^c U_i^2 \end{bmatrix}. \quad (4)$$

The superscripts 1 and 2 represent two different simulations with the loads set as a theoretical unflanged radiation impedance and the characteristic impedance, respectively. The closed mouthpiece input impedance can be calculated as $Z_{closed} = T_{11}/T_{21}$, which agrees well with that calculated by the FE model as shown in Fig. 2. Comparing the input impedance calculated by the TM model to that calculated by the FE model, the largest discrepancies in the resonance peak magnitudes and frequencies are 0.7 dB and 0.2%, respectively. Since the wall admittance is applied to the solid boundaries of the FE model, viscothermal losses are intrinsically included in the derived TM model. However, because the TM model is derived from the FE simulation with specific temperature and corresponding physical variables, viscothermal losses are immutable once the TM is derived.

To enable the application of the TM mouthpiece model to other studies, the TM is approximated with four 10th-order polynomials to fit all complex matrix elements T_{ij} up

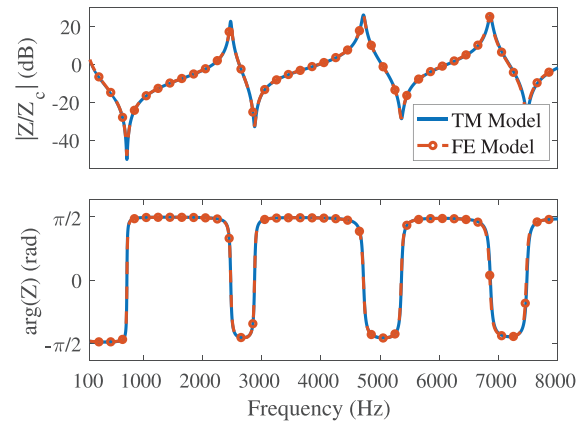


FIG. 2. (Color online) The comparison of the modulus (top) and argument (bottom) of mouthpiece input impedances computed by the FE model and the TM model.

to 8 kHz.¹ The estimation errors, defined as $E_{ij} = ||T_{ij} - T_{ij}^{poly}||_2 / ||T_{ij}||_2$, for all elements are less than 0.5%, where T_{ij}^{poly} are approximated matrix elements. The polynomial approximation is available online (Computational Acoustic Modeling Laboratory, 2018).

III. MODEL VALIDATIONS

A. Input impedance measurements

The FE and TM models were validated by comparisons with measured input impedances. The acoustic impedance measurements were performed with a custom-build multi-microphone system (Lefebvre and Scavone, 2011) consisting of six microphones along a cylindrical impedance head of 6.5 mm radius, providing a cutoff frequency slightly greater than 15 kHz. Three resonance-free calibration loads were used similar to the ones described by Dickens *et al.* (2007), including a quasi-infinite impedance, an almost purely resistive impedance, and an unflanged pipe radiation load. For this paper, the input impedances of an alto saxophone mouthpiece, a 40 cm-long truncated cone made of carbon fibre (3° taper angle), and the combination of the mouthpiece and the truncated cone (the mouthpiece-cone system) were measured. To connect the mouthpiece to the impedance head, an adapted structure having the same inner geometry as the mouthpiece was designed and 3D-printed for the measurement. The surface of the reed and the side slits were closed by the walls in the adapter, with only a small rectangular tip window open to the impedance head.

When measuring the input impedance of the mouthpiece alone, the mouthpiece was closed by a 3D-printed block that shortened the mouthpiece inner length by 1 cm. For consistency, the truncated cone was inserted the same distance into the mouthpiece when measuring the mouthpiece-cone system.

The input impedances of the truncated cone, closed mouthpiece, and mouthpiece-cone system are shown in Fig. 3. Compared to the truncated cone, the frequencies of the first few impedance peaks of the mouthpiece-cone system are lower because the mouthpiece lengthens the instrument. The

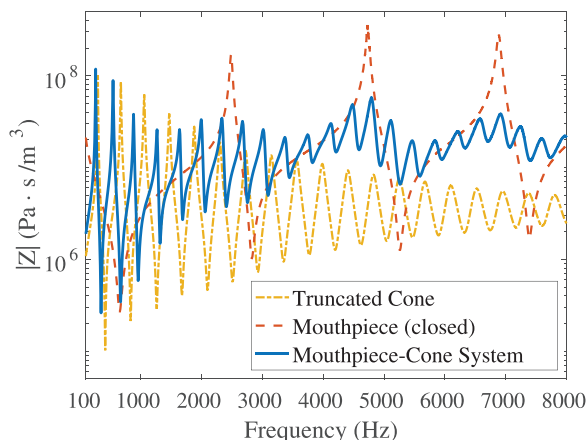


FIG. 3. (Color online) The measured input impedances of the truncated cone, the closed mouthpiece, and the mouthpiece-cone system.

mouthpiece also modulates the input impedance of the resonator by amplifying it around the mouthpiece’s resonance frequencies. This indicates a similar role as that played by a trumpet mouthpiece (Caussé *et al.*, 1984), which helps explain the brightness contributed by the mouthpiece.

B. Validation of the FE model

The FE model of the mouthpiece was validated by comparing the simulated closed mouthpiece input impedance with the measured one, as shown in Fig. 4. A frequency-domain phase correction was applied to the measured data to compensate for sub-sample time delay discrepancies. Good agreement is achieved up to 15 kHz with maximum discrepancies of 1.8 dB in the magnitudes and 0.5% in the frequencies between the resonance peaks of the measured and simulated input impedances. There are relatively larger discrepancies around the anti-resonant frequencies than the resonant frequencies, which is mainly attributed to the discontinuity between the impedance head and the mouthpiece tip window and might be potentially mitigated by taking into account the influence of higher-order modes using the multimodal method (van Walstijn *et al.*, 2005). The onset of

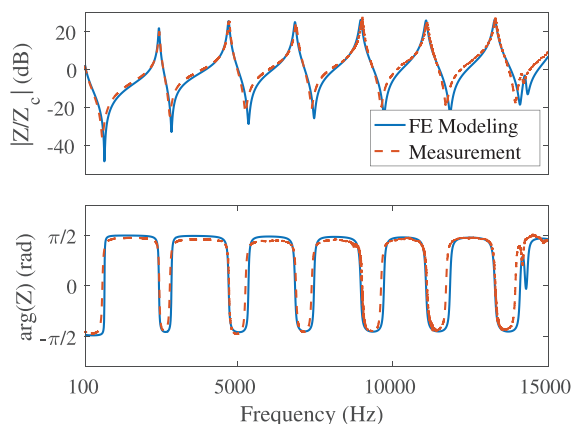


FIG. 4. (Color online) The measured input impedance of the closed mouthpiece and that simulated using the FE model.

the higher-order mode can be observed around 1.4 kHz in both the measured and FE-modeled input impedances. This corresponds to the cutoff frequency of the mouthpiece, above which non-planar modes are observed in the pressure iso-surface plot in COMSOL. It is worth noting that the cutoff frequency of the mouthpiece is larger than 12.7 kHz, the cutoff frequency of an ideal cylindrical pipe with a radius equal to that of the mouthpiece shank (the cylindrical part of the mouthpiece into which a resonator is inserted).

C. Validation of the TM model

The mouthpiece-cone system was used to validate the TM model derived in Sec. II B. The measured input impedance of the conical frustum Z_{cone} was coupled to the TM mouthpiece as a load impedance. Since the diameter of the cone is different from that of the mouthpiece shank, there exists a discontinuity at the interface. Because the diameter difference is small, the influence of the non-propagating modes on the propagating mode is neglected, and the acoustic impedances on the two sides of the junction are assumed equal to each other. However, the discontinuity, as illustrated in Fig. 5, should be carefully treated when using the normalized acoustic impedance $\tilde{Z} = Z/Z_c$ in the calculations. The normalized impedance on the right of the junction is written as $\tilde{Z}_2 = \tilde{Z}_1 S_2/S_1$, where S_1 and S_2 are the cross section areas on the left and right of the junction, respectively.

The input impedance of the mouthpiece-cone system can then be calculated with the following equation:

$$\tilde{Z}_{mc} = \frac{T_{11} + T_{12}/\tilde{Z}_2}{T_{21} + T_{22}/\tilde{Z}_2}. \quad (5)$$

The comparison between the measured and calculated input impedances is shown in Fig. 6. The calculated input impedance generally matches the measured one, with the largest peak magnitude discrepancy of 1.8 dB and the largest peak frequency deviation less than 1%. As mentioned before, the discrepancies around the anti-resonances are relatively larger, which is due to the measurement error caused by the discontinuity between the impedance head and the mouthpiece tip window.

IV. ACOUSTIC COMPARISON BETWEEN DIFFERENT MOUTHPIECE MODELS

A. Mouthpiece coupled to a truncated cone

The TM mouthpiece model can be compared to two previously reported mouthpiece representations, i.e., the

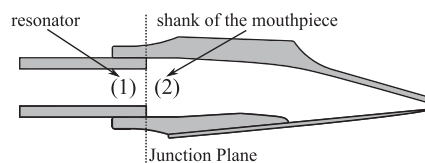


FIG. 5. An illustration of the junction between the mouthpiece and the resonator.

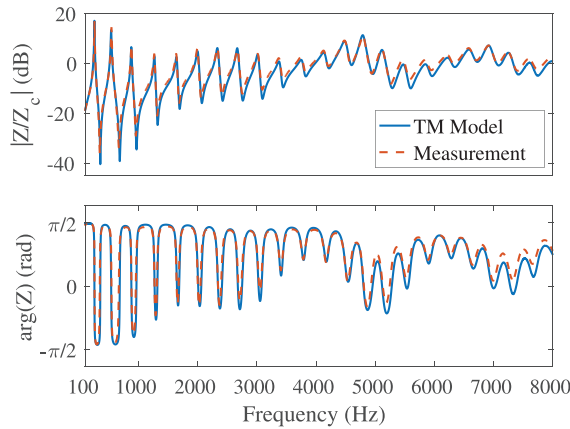


FIG. 6. (Color online) The measured input impedance of the mouthpiece-cone system and that calculated with the TM model using Eq. (5).

cylindrical mouthpiece model and the lumped mouthpiece model. For each of the mouthpiece representations, the input impedance of a combined mouthpiece-cone system is calculated using the input impedance of the truncated cone measured in Sec. III as the load impedance.

The cylindrical mouthpiece model takes the mouthpiece as a pure cylinder that has the same volume V_m as the missing part of the truncated cone. In this paper, the cylindrical mouthpiece is modeled based on the TM representation as

$$\mathbf{T}_{cyl} = \begin{bmatrix} \cosh(\Gamma L) & Z_c \sinh(\Gamma L) \\ Z_c^{-1} \sinh(\Gamma L) & \cosh(\Gamma L) \end{bmatrix}, \quad (6)$$

where Γ depends on the acoustic constants of the air (Chaigne and Kergomard, 2016) and includes the wall losses due to viscothermal effects.

For consistency, the radius of the cylinder is chosen to be equal to that of the mouthpiece shank S_2 so that the length of the mouthpiece $L = V_m/S_2$ is fixed. The input impedance of the mouthpiece-cone system \tilde{Z}_{mc} is calculated using Eq. (5) by substituting \mathbf{T} with \mathbf{T}_{cyl} .

The lumped mouthpiece model approximates the mouthpiece as an acoustic compliance $C_m = V_m/(\rho c^2)$ in parallel with the impedance of the resonator. This lumped representation is often sufficient for low frequencies, where the wavelength is large compared to the characteristic length of the mouthpiece. Taking the same load impedance Z_2 used with the other mouthpiece models, the input impedance of the mouthpiece-cone system with a lumped mouthpiece is calculated as

$$Z_{mc}^{lumped} = \frac{1}{\frac{1}{Z_2} + j\omega C_m}. \quad (7)$$

The input impedances of mouthpiece-cone systems with different mouthpiece models are compared with the measurement in Fig. 7. The calculations with the TM mouthpiece model result in the best match to the measured input impedance compared to the other two mouthpiece representations. Because all three mouthpiece models have the

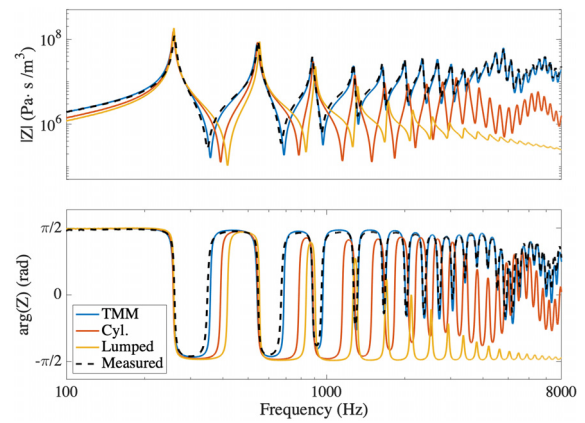


FIG. 7. (Color online) The measured input impedance of the mouthpiece-cone system and that calculated using the TM mouthpiece model (TMM), the cylindrical mouthpiece model (Cyl.) and the lumped mouthpiece model (Lumped).

same mouthpiece volume, they have a similar behavior at low frequencies where the lumped model assumption is valid. However, the performance of the lumped mouthpiece degrades quickly as it shunts high-frequency components. The high-frequency characteristics of the cylindrical mouthpiece model show significant discrepancies from the measured and TM mouthpiece responses because of the oversimplified geometric approximation. Derived from the FE model, the TM mouthpiece intrinsically contains the complex geometry information of the mouthpiece, which provides advantages in preserving the high-frequency structure over the other models.

B. Mouthpiece coupled to an alto saxophone

Previous input impedance $[Z(\omega) = P(\omega)/U(\omega)]$ and radiation transfer function $[E(\omega) = T(\omega)/U(\omega)]$ measurements of an alto saxophone (without mouthpiece) made by Maestre *et al.* (2018) were used to investigate the coupling of the different mouthpiece models with an alto saxophone. $P(\omega)$ and $T(\omega)$ are the frequency-domain mouthpiece pressure and radiated pressure, respectively, and $U(\omega)$ is the volume flow rate at the entrance of the resonator in the frequency domain. As with the mouthpiece-cone system, coupled responses were obtained with the measurements as load impedances. In the junction between the shank of the mouthpiece and the neck of the saxophone, there is a discontinuity that was accounted for by multiplying the measured saxophone body input impedance by the cross section area ratio S_2/S_1 so that we were able to obtain the impedance on the mouthpiece side of the junction $\tilde{Z}_2 = \tilde{Z}_1 S_2/S_1$. Similarly, the radiation transfer function was also multiplied by the same factor so that $\tilde{E}_2 = \tilde{E}_1 S_2/S_1$. Input impedances of the entire instrument can be calculated using either Eq. (5) for the TM mouthpiece and cylindrical mouthpiece or Eq. (7) for the lumped mouthpiece. For the cylindrical mouthpiece and the TM mouthpiece, the radiation transfer function can be derived as follows using the TM elements:

$$\tilde{E}_{sax} = \frac{\tilde{E}_2}{T_{21}\tilde{Z}_2 + T_{22}} \quad (8)$$

For the lumped mouthpiece, the radiation transfer function is calculated as

$$E_{sax}^{lumped} = \frac{\tilde{E}_2\tilde{Z}_{sax}^{lumped}}{\tilde{Z}_2} \quad (9)$$

As an example, the input impedances and the radiation transfer functions with and without the TM mouthpiece are shown in Fig. 8 for the note B^b4 (written).

The mouthpiece helps tune the fundamental frequency and the harmonics by completing the truncated cone of the saxophone body. To compare the influence of the different mouthpiece representations on the alignment of the impedance peaks across the entire playing range, each mouthpiece model was tuned separately when coupled with the measurement for the F4 (written) fingering by adjusting the mouthpiece volume to align the first input impedance peak to the corresponding equal-tempered scale frequency.

As shown in Fig. 9, the deviations (in cents) between the frequency of the first or second peak of the input impedance and the equal-tempered scale frequency of each note are compared among different fingerings with and without different mouthpiece models. Comparisons are made to the first input impedance peak for first register notes (below D5) and to the second peak for the remaining (second register) notes. For the body of the saxophone alone (without mouthpiece), the deviation is large and generally increases with the fundamental frequency within each register. All the mouthpiece models help reduce such deviation, though the tuning performance varies from note to note. The TM mouthpiece performs similarly to the other two mouthpiece models in the first register, while it shows the least deviation in the second register.

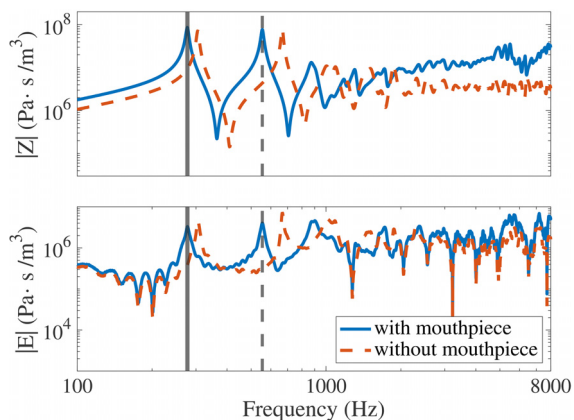


FIG. 8. (Color online) Comparisons of the input impedance and radiation transfer function with (solid lines) and without (dashed lines) the TM mouthpiece for the note B^b4 (written). The vertical solid and dashed lines correspond to the equal-tempered scale frequencies of the first and second harmonics of the note, respectively. The input impedance and radiation transfer function with the TM mouthpiece are calculated using Eqs. (5) and (8), respectively.

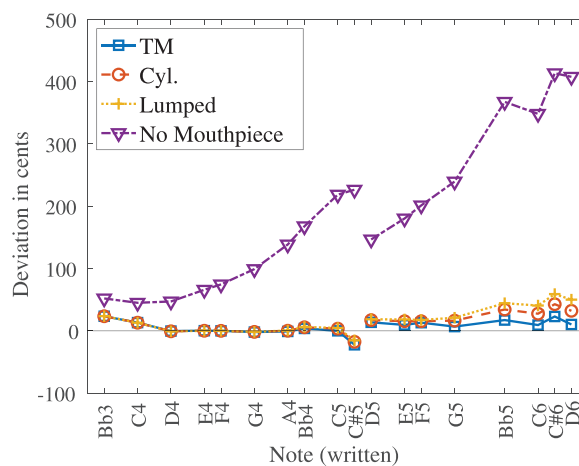


FIG. 9. (Color online) The deviation in cents between the first or second input impedance peak and the equal-tempered scale frequency of different notes.

Following the definition of the inharmonicity parameter used by Gilbert *et al.* (2019), the inharmonicity for the notes of the first register was characterized as $I = (f_2 - 2f_1)/2f_1$, where f_1 and f_2 are the two lowest resonance frequencies of the input impedance. The comparison of the inharmonicities between the saxophone with different mouthpiece models is displayed in Fig. 10, showing that the input impedance peaks of the saxophone with the TM mouthpiece are more harmonically aligned than the others.

More comparisons between the saxophones with different mouthpiece models for the note B^b4 (written) are shown in Fig. 11, including the input impedance, normalized input impedance, reflection function, and radiation transfer function. All mouthpieces have the same volume in this comparison, and as expected, they have similar behavior in the lower-frequency range. The magnitude and the frequency of the first peak match each other very well, while the difference between the second peak is more significant. Comparing the normalized input impedances, magnitude differences are readily apparent. This is

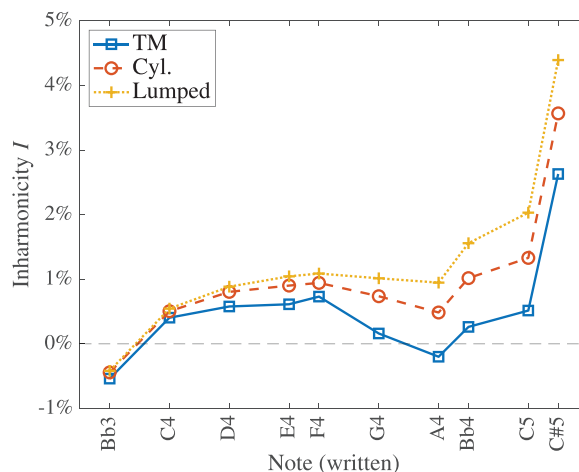


FIG. 10. (Color online) Input impedance peak inharmonicities for the different mouthpiece representations.

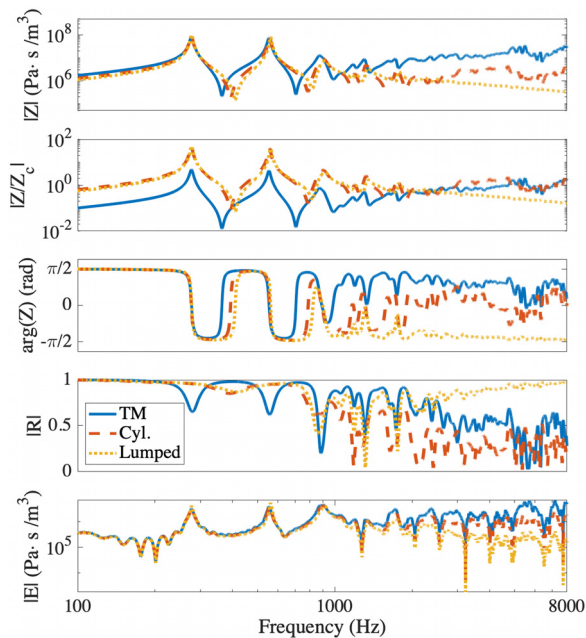


FIG. 11. (Color online) Comparisons (from top to bottom) of the modulus of the physical input impedances, the modulus of the normalized input impedances, the argument of the normalized input impedances, the reflection functions, and the radiation transfer functions between the TM mouthpiece (solid lines), the cylindrical mouthpiece (dashed lines), and the lumped mouthpiece (dotted lines) coupled with the measured impedance of the alto saxophone resonator for the note B[♭]4 (written).

because the impedance is normalized by values of Z_c that are calculated with different cross section areas for different mouthpiece models. For the cylindrical and lumped mouthpieces, the shank cross section area is used (see Fig. 5). However, the TM mouthpiece results are normalized by the cross section area at the mouthpiece tip, which is much smaller than the shank area. At higher frequencies, the input impedance magnitudes of the TM mouthpiece and the cylindrical mouthpiece converge toward the specific impedance (or a normalized value of 1). However, due to the increase in the acoustic admittance used in the lumped model, the input impedance magnitude continues to decrease, which causes the reflection function to approach 1 as the frequency increases. Such a behavior can be especially problematic in the context of sound synthesis, as mentioned by Kergomard *et al.* (2016), so a pre-processing must be applied to force the reflection function toward zero, as discussed in Sec. V.

The differences in the magnitude level of the normalized input impedance also lead to differences in the magnitudes of the reflection function $R = (\tilde{Z} - 1)/(\tilde{Z} + 1)$. As can be seen from its definition, the magnitude of the reflection function will have minima around frequencies where $\tilde{Z} \approx 1$. Because the input impedance magnitude of the TM mouthpiece system is generally lower than that of the other two mouthpiece models and the magnitudes of the first two peaks are just above 1, the $|R|$ -plot of the TM mouthpiece has extra dips around 2000–4000 Hz, and their positions do not correspond with those of the other two models.

Finally, the comparison of the radiation transfer function shows that all three different mouthpiece models have a similar behavior at the low frequencies, and the high-frequency characteristics of the TM mouthpiece are more significant compared to those of the other mouthpiece models. This is consistent with the discussion about the input impedance comparison.

V. SOUND AND DYNAMICS COMPARISON BETWEEN DIFFERENT MOUTHPIECE MODELS

This section describes the synthesis of alto saxophone sounds using different mouthpiece models and measured saxophone impedances in order to analyze the influence of different mouthpiece models on the nonlinear dynamics and properties of the rendered sound. Based on the work by Maestre *et al.* (2018), the saxophone was represented by the classic three-equation single-reed instrument model (Chaigne and Kergomard, 2016), which was discretized based on a combination of three different schemes (Guillemain *et al.*, 2005; Maestre and Scavone, 2016; Scavone and Smith, 2006). As previously described, the different mouthpiece models were coupled to measured input impedance and radiation transfer functions of an alto saxophone. From this frequency-domain data, we fit recursive parallel filters that jointly represented the mouthpiece and the resonator as an efficient digital filter that was used for audio synthesis for a subsequent analysis of dynamics and sound properties. The results of the note B[♭]4 (written) were taken as an example to quantitatively compare the performances of different mouthpiece models with the discussion of possible explanations for their differences in sound characteristics and dynamics behavior.

A. The synthesis model

The standard three-equation single-reed instrument model comprises three unknowns: the mouthpiece pressure p , the volume velocity u , and the reed tip displacement y away from the equilibrium position. Dimensionless variables are used in the governing equations as

$$\tilde{p} = \frac{p}{p_M}, \quad \tilde{u} = Z_c \frac{u}{p_M}, \quad \tilde{y} = \frac{y}{H}, \quad (10)$$

where p_M is the mouth pressure at which the reed channel is closed, Z_c is the characteristic impedance at the input of the resonator, and H is the distance at equilibrium from the tip of the reed to the lay of the mouthpiece. For the sake of simplicity, all the tildes are subsequently omitted.

The pressure-controlled reed is modeled by a single-degree-of-freedom damped oscillator that is governed by the following equation:

$$\frac{1}{\omega_r^2} \frac{d^2 y}{dt^2} + \frac{q_r}{\omega_r} \frac{dy}{dt} + y = -\Delta p, \quad (11)$$

where $\omega_r = 2\pi f_r$ with f_r being the reed resonance frequency, and q_r is the reed damping coefficient. The variable

$\Delta p = \gamma - p$ is the pressure difference between the mouth pressure γ and the pressure in the mouthpiece p .

The linear resonator, composed of the mouthpiece and the saxophone, is modeled based on the input impedance of the entire system,

$$Z(\omega) = \frac{P(\omega)}{U(\omega)}. \tag{12}$$

The nonlinearity of the saxophone is governed by the Bernoulli flow equation:

$$u = \begin{cases} \zeta(1+y)\text{sign}(\gamma-p)\sqrt{|\gamma-p|}, & 1+y \geq 0, \\ 0, & 1+y < 0, \end{cases} \tag{13}$$

where $\zeta = Z_c w H \sqrt{2/(\rho p_M)}$, with w the reed channel width.

Equations (11)–(13) compose the governing equations of the saxophone model, which need to be discretized for the time-domain sound synthesis.

The discretization of the reed model is performed by way of the bilinear transform (Scavone and Smith, 2006), leading to

$$\frac{Y(z)}{\Delta P(z)} = \frac{-4\omega_r^2 z^{-1}}{a_0 + 2(\omega_r^2 - \alpha^2)z^{-1} + (\alpha^2 - g_r \alpha + \omega_r^2)z^{-2}}, \tag{14}$$

where $g_r = q_r/\omega_r$, $a_0 = \alpha^2 + g_r \alpha + \omega_r^2$ and $\alpha = \omega_r / \tan(\omega_r/2f_s)$ is the bilinear transform constant that controls the frequency warping and is defined to match the reed resonance frequency between the continuous and discrete domains.

The input impedance $Z(\omega)$ is modeled as a recursive parallel filter (Maestre and Scavone, 2016; Maestre et al., 2017). Akin to a discretized modal expansion, its resonant behavior is conveyed by a number of parallel one-zero, two-pole resonators in the z -domain:

$$Z(z) = \sum_{n=1}^N (b_{0,n} + b_{1,n}z^{-1})H_n(z), \tag{15}$$

where

$$H_n(z) = \frac{1 - z^{-1}}{(1 - p_n z^{-1})(1 - \bar{p}_n z^{-1})}, \tag{16}$$

with p_n and \bar{p}_n being a pair of complex conjugate poles.

As described by Maestre et al. (2018), the impedance digital filter $Z(z)$ can be decomposed into a linear form

$$Z(z) = B_0 + z^{-1}V(z), \tag{17}$$

where $B_0 = \sum_{n=1}^N b_{0,n}$ is a constant and $V(z)$ is the collection of the remaining terms depending only on the history. The pressure is then obtained by discretizing Eq. (12) and substituting Eq. (17), leading to a time-domain form

$$p[n] = B_0 u[n] + q[n], \tag{18}$$

where $q[n]$ only depends on the history of $u[n]$, i.e., on $u[n-k]$ with $k \geq 1$.

By substituting Eq. (18) into the discrete version of Eq. (13), the volume flow rate $u[n]$ can be solved explicitly as (Guillemain et al., 2005)

$$u[n] = \begin{cases} \frac{1}{2} \text{sign}(\gamma - q[n]) \sqrt{(-B_0 w[n]^2 + w[n] \sqrt{(B_0 w[n])^2 + 4|\gamma - q[n]|})} & 1 + y[n] \geq 0, \\ 0, & 1 + y[n] < 0, \end{cases} \tag{19}$$

where $w[n] = \zeta(1 + y[n])$. Afterward, $p[n]$ can be updated using Eq. (18).

To obtain the radiated sound, we employed again the scheme proposed by Maestre et al. (2018), which jointly approximates the input impedance $Z(\omega)$ and the radiation transfer function $E(\omega)$ as a single set of recursive digital filters in parallel form. As in the case of the impedance, this leads to a time-domain expression for the radiated sound pressure as

$$t[n] = D_0 u[n] + g[n], \tag{20}$$

where D_0 is constant and $g[n]$ only depends on $u[n-k]$, with $k \geq 1$.

Thus, to summarize, the acoustic pressure $p[n]$, flow rate $u[n]$, and radiated sound pressure $t[n]$ were computed as follows:

- (1) Update the reed position $y[n]$ using Eq. (14).
- (2) Update $q[n]$ and $g[n]$ in Eq. (18) and Eq. (20), correspondingly, based on previous samples of the flow rate $u[n-k]$ with $k \geq 1$.
- (3) Explicitly solve the flow rate in the mouthpiece $u[n]$ using Eq. (19).
- (4) Calculate the mouthpiece pressure $p[n]$ and the radiated pressure $t[n]$ using Eqs. (18) and (20), respectively.
- (5) Go back to step 1.

The number of parallel sections N depends on the fingerings and the mouthpiece models and was manually selected. A higher-note fingering normally has a smaller N than that of a lower-note fingering, for it involves less prominent modes. For a resonator with $N = 32$ parallel sections and a sampling frequency of 48 kHz, this model ran at a

speed more than 30 times faster than real-time on one logical core of a laptop computer.

B. Fitting of the input impedance and the radiation transfer function

To design the digital filters corresponding to the impedance model and the radiation model, we employed the nonlinear optimization described by *Maestre et al. (2018)*. The sound synthesis model was designed to run at a standard audio sample rate of 48 kHz. Some preprocessing was performed before fitting the digital filter coefficients. For the cases of TM mouthpiece and cylindrical mouthpiece representations, the target normalized input impedance magnitude above 8 kHz was set to 1, with a cross-fade region from 7 to 8 kHz. This assumes that no sound is reflected from the end of the instrument above 8 kHz. For the lumped mouthpiece representation, the target normalized input impedance magnitude was cross-faded to 1 in the region from 2 to 3 kHz, for reasons noted in Sec. IV. For all three mouthpiece models, the magnitude of the radiation transfer function was set to -40 dB above 8 kHz, as this response exhibited some noise at higher frequencies due to limitations of the measurement space.

The fittings of the input impedance and the radiation transfer function are shown in Fig. 12. For the lumped mouthpiece model, $N = 14$ parallel sections were used, while $N = 32$ for the cylindrical and the TM mouthpiece models.

C. Analysis of nonlinear dynamics and sound properties

The sound of the saxophone was synthesized at the sampling frequency 48 kHz for the note B[♭]4 with different mouthpiece models. The resonance frequency of the reed

was $f_r = 1500$ Hz, the damping factor was $q_r = 1.5$, the stiffness of the reed was $k_r = 8 \times 10^6$ Pa/m, the density was $\rho = 1.18$ kg/m³, and the speed of sound was defined as 347.23 m/s. The width of the mouthpiece tip window was $w = 12$ mm, and the equilibrium height of the reed channel was $H_0 = 0.8$ mm. The reed parameters were initially chosen based on values provided in the literature (*Colinot et al., 2020; Petersen et al., 2019*), though they were subsequently modified so that the synthesized sounds of different mouthpiece models were in the same regimes. These values correspond to $\zeta = 0.3$ in Eq. (13) for the lumped and cylindrical mouthpiece models, which falls into the typical range $\zeta \in [0.1, 1]$ (*Kergomard et al., 2016*).

The synthesis was performed using a linearly varying mouth pressure with a fixed slope $k = 0.01$. The normalized mouth pressure γ either increased from 0 to 3 or decreased from 1.2 to 0. The comparisons of the bifurcation diagrams, fundamental frequencies, and spectral centroids exhibited by different mouthpiece models are shown in Fig. 13 for the increasing and decreasing mouth pressure profiles.

Unlike the traditional bifurcation diagram generated by solving a nonlinear system theoretically (*Dalmont et al., 2000*) or numerically (*Colinot et al., 2020*), the one shown at the top of Fig. 13 was obtained by extracting the envelope of the synthesized mouthpiece pressure p , as has been used by *Colinot et al. (2019)*. Though it cannot show all bifurcation branches or types, this diagram presents the stable solutions from which it is possible to identify the different dynamics thresholds, including the oscillation threshold, extinction threshold, inverse oscillation threshold, and inverse extinction threshold, and compare them between different mouthpiece models. In addition, one may notice the sudden jump taking place in the bifurcation diagram along the lower envelope around $\gamma = 1.5$, which corresponds to the point that the oscillation changes from the Helmholtz

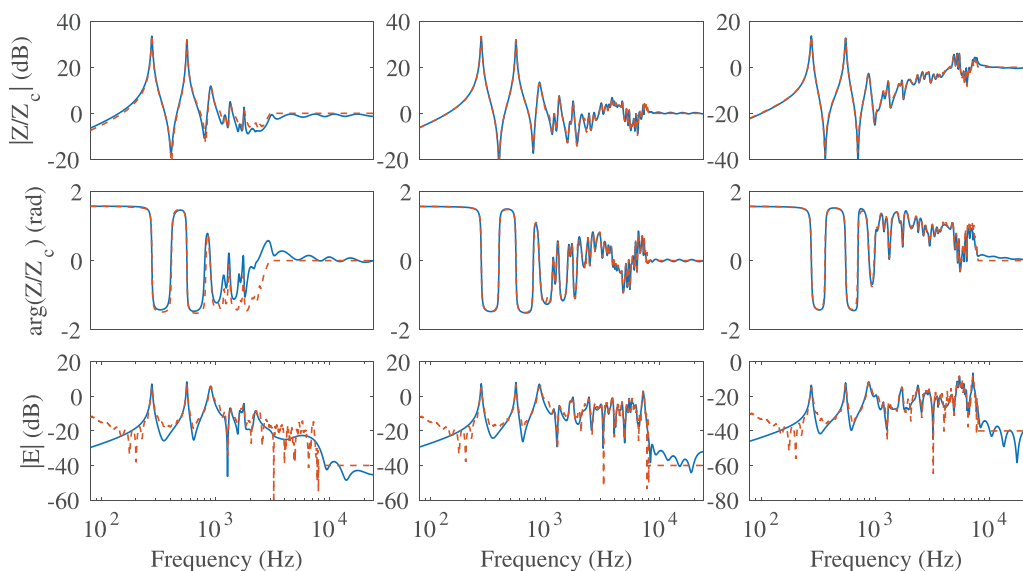


FIG. 12. (Color online) The fitting of the modulus (top) and argument (middle) of the impedance and the radiation transfer function (bottom) of the lumped mouthpiece (left), cylindrical mouthpiece (center), and TM mouthpiece (right). In each plot, dashed lines (red) and solid lines (blue) are used to represent the original data and the model, respectively.

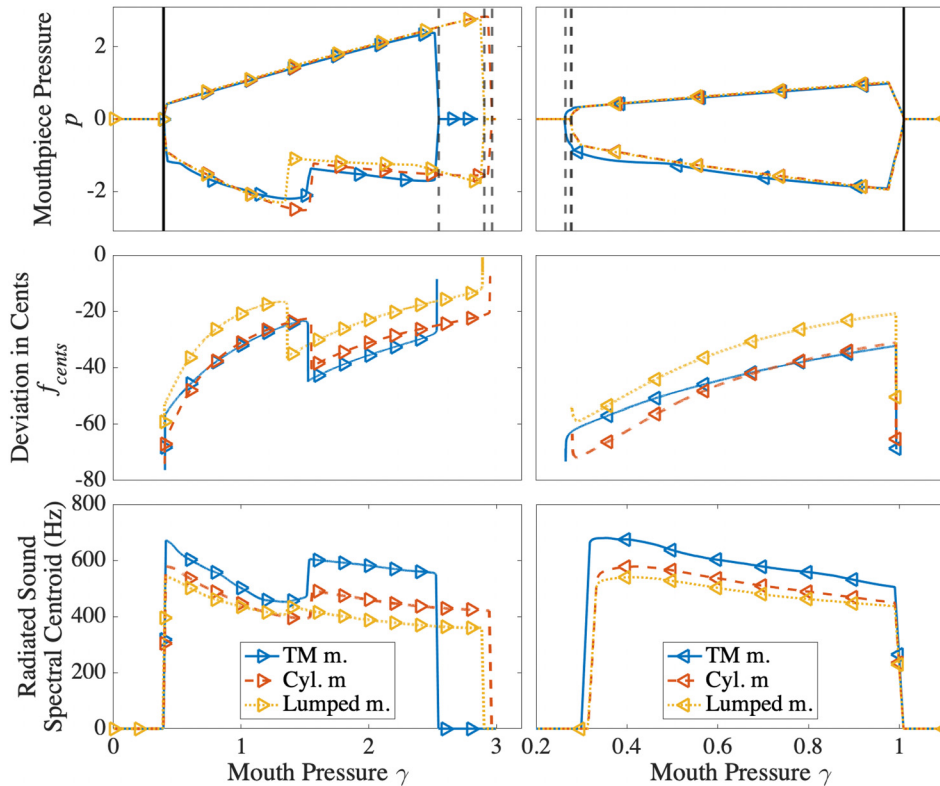


FIG. 13. (Color online) Comparisons of the bifurcation diagrams (top), playing frequencies (middle), and radiated sound spectral centroid (bottom) for increasing (left) and decreasing (right) mouth pressure profiles. The (inverse) oscillation thresholds and (inverse) extinction thresholds are shown in the bifurcation diagrams as vertical solid and dashed lines, correspondingly.

motion to the inverted Helmholtz motion, as discussed by Dalmont (2007). While the overall characteristics remain similar, the main differences between mouthpiece models revolve around the extinction threshold identified in the bifurcation diagram. The thresholds where the regime changes from Helmholtz motion to inverted Helmholtz motion also vary among different mouthpiece models. The difference in thresholds is partially explained by the inharmonicity difference as shown in Fig. 10. However, though inharmonicity of impedance peaks has been shown to influence dynamics (Dalmont *et al.*, 1995; Doc and Vergez, 2015; Gilbert *et al.*, 2019), its impact on different oscillation thresholds is still unclear.

The playing frequency f_p was also compared based on its deviation from the frequency of the first peak of the input impedance f_1 ,

$$f_{cents} = 1200 \log_2 \left(\frac{f_p}{f_1} \right), \quad (21)$$

and the difference can be as large as 15 cents between mouthpiece models. Such differences are partially contributed by the inharmonicity among different mouthpiece models as discussed in Sec. IV B (Coyle *et al.*, 2015; Dalmont *et al.*, 1995; Gilbert *et al.*, 2019).

The spectral centroids of the radiated sound were compared as well. As shown at the bottom of Fig. 13, the TM mouthpiece has the highest spectral centroid, mainly due to its more accurate representation of higher-frequency characteristics as indicated in the input impedance and the radiation transfer function.

The waveforms of the pressure inside the mouthpiece of two different regimes are shown in Fig. 14. The mouthpiece pressure waveforms for the three different models are generally similar to each other, though the TM mouthpiece result displays the largest fluctuation, especially when the reed is closed (around the valleys of the pressure waveform). This can be traced to the discontinuity in the flow model as the reed channel starts to close and the fact that the TM mouthpiece model reflects more high-frequency components.

When $\gamma = 2$, the saxophone is oscillating under the inverted Helmholtz motion. It is interesting to see that the cylindrical mouthpiece has a more similar waveform to the TM mouthpiece than to the lumped mouthpiece model. This could indicate that under the inverted Helmholtz motion, where the closing phase of the reed channel is longer than the opening phase, the inertance of the mouthpiece plays an important role in determining the waveform. However, such an assumption needs to be further tested before a conclusion can be drawn.

Finally, the so-called bifurcation delay was quantitatively compared among different mouthpiece models. The bifurcation delay was first proposed in the context of the clarinet by Bergeot *et al.* (2014) and is defined by the difference between the theoretical oscillation threshold and the dynamic threshold simulated under dynamic conditions (as in our experiments). In practice, the bifurcation delay is calculated as $BD = P_{mdt} - P_{mst}$. P_{mst} is the minimum value of a static blowing pressure above which an instability can emerge. P_{mdt} is the dynamic oscillation threshold where the periodic oscillation occurs when the mouth pressure increases. However, the theoretical oscillation threshold is

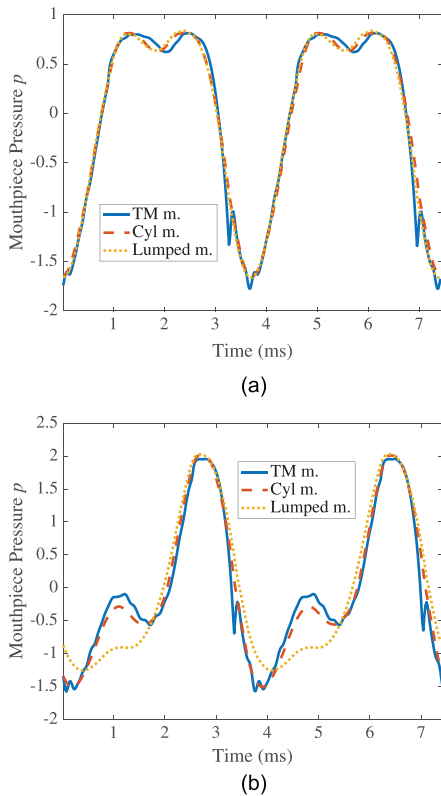


FIG. 14. (Color online) The comparison of the waveforms among three mouthpiece models when (a) $\gamma = 0.8$ and (b) $\gamma = 2$.

nearly impossible to estimate for a real instrument. As shown in the results by [Bergeot et al. \(2014\)](#), decreasing the mouth pressure changing rate k will make the measured inverse extinction threshold closer to the theoretical static oscillation threshold. Based on this, P_{mst} was set to the inverse extinction threshold with the smallest pressure change rate of $k = 0.01$. The comparison of BD and its changes with k are displayed in Fig. 15. For a better sense of the difference, the pressure is shown in pascals rather than dimensionless pressure in this figure.

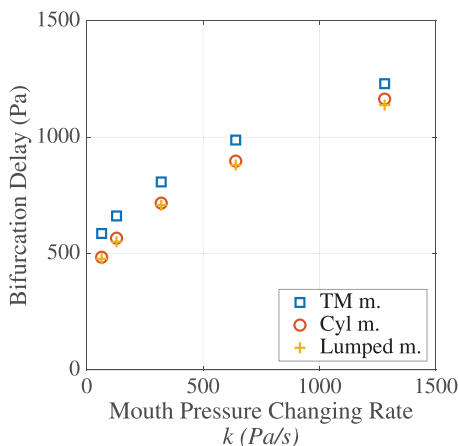


FIG. 15. (Color online) The comparison of the bifurcation delays with different mouth pressure changing rate k .

VI. CONCLUSION AND PERSPECTIVES

In this paper, we proposed an acoustic model of the mouthpiece as a TM. The TM model was derived from a FE mouthpiece model and was validated by comparing the calculated input impedance of a mouthpiece-cone system with measurements. The same measured input impedance was also used to compare calculated results using lumped and cylindrical mouthpiece models. The TM mouthpiece model was shown to be the most accurate representation among all three models, providing also the highest degree of fidelity in the high-frequency region.

Using a sound synthesis model based on parallel recursive filters, the three different mouthpiece models were coupled to the same alto saxophone, and a comparison was performed in terms of the fundamental frequency, inharmonicity, dynamics threshold, playing frequency, spectral centroid, pressure waveform, and bifurcation delay. Different mouthpiece models clearly show varying behaviors that can be explained by differences in their inharmonicity and high-frequency characteristics. In this paper, basic comparisons were aimed at demonstrating differences in terms of a number of acoustical and dynamical features in simulated played conditions, and we leave a detailed analysis of other features, such as the influence of inharmonicity or higher modes on the dynamics, for future studies.

The proposed TM model is flexible and appropriate for multiple applications as the TM provides an efficient way to model the mouthpiece while being accurate enough to retain the complex mouthpiece geometry information. The TM model, which could be applied to other instruments, such as the clarinet, can be coupled to different resonators by taking either the measured or calculated resonator input impedance as the load impedance, and this can be useful for instrument prototyping purposes. It should also be straightforward to use the TM mouthpiece model in a variety of sound synthesis schemes, leading to a better simulation of both high- and low-frequency regions. In that regard, a potential application is to transform the TM scheme into a time-domain scattering representation, such as those used with digital waveguide models ([Scavone, 1997](#); [van Walstijn, 2002](#)).

The TM model can characterize acoustical influences on the sound and dynamics behavior of the saxophone. However, it is important to note that both dynamics and the sound are influenced by aeroacoustic aspects, e.g., the vortex sound and the turbulence, as well, which are not addressed by this model.

ACKNOWLEDGMENTS

This research is supported by the Natural Sciences and Engineering Research Council of Canada and the Centre for Interdisciplinary Research in Music Media and Technology at McGill University.

¹The TM mouthpiece model derived from the FE model is accurate to as high as the mouthpiece's cutoff frequency around 14 kHz, though only the part below 8 kHz was validated in this paper.

- Andrieux, B., Cottier, J., Selmer, J., and Gibiat, V. (2016). "Caractérisation de l'impédance acoustique du couple bec-instrument par l'utilisation d'une méthode mixte mettant en jeu le calcul par éléments finis et la mesure par la méthode TMTC," in *Proceedings of Congrès Français D'Acoustique*, April 11–15, Le Mans, France.
- Andrieux, B., Gibiat, V., and Selmer, J. (2014). "Modeling of a woodwind mouthpiece using a finite-element method and characterization of its acoustic input impedance," in *Proceedings of the International Symposium on Music Acoustics (ISMA) 2014*, July 7–12, Le Mans, France.
- Avanzini, F., and van Walstijn, M. (2004). "Modelling the mechanical response of the reed-mouthpiece-lip system of a clarinet. Part I. A one-dimensional distributed model," *Acta Acust. United Acust.* **90**(3), 537–547.
- Ayers, R. D., Eliason, L. J., and Mahgerefteh, D. (1985). "The conical bore in musical acoustics," *Am. J. Phys.* **53**(6), 528–537.
- Benade, A. H. (1990). *Fundamentals of Musical Acoustics*, 2nd ed. (Dover, New York).
- Bergeot, B., Almeida, A., Gazengel, B., Vergez, C., and Ferrand, D. (2014). "Response of an artificially blown clarinet to different blowing pressure profiles," *J. Acoust. Soc. Am.* **135**(1), 479–490.
- Caussé, R., Kergomard, J., and Lurton, X. (1984). "Input impedance of brass musical instruments—comparison between experiment and numerical models," *J. Acoust. Soc. Am.* **75**(1), 241–254.
- Chaigne, A., and Kergomard, J. (2016). *Acoustics of Musical Instruments* (Springer-Verlag, New York).
- Chen, J.-M., Smith, J., and Wolfe, J. (2009). "Saxophone acoustics: Introducing a compendium of impedance and sound spectra," *Acoust. Aust.* **37**(1), 18–23.
- Colinot, T., Guillemain, P., Vergez, C., Doc, J.-B., and Sanchez, P. (2020). "Multiple two-step oscillation regimes produced by the alto saxophone," *J. Acoust. Soc. Am.* **147**(4), 2406–2413.
- Colinot, T., Guillot, L., and Kergomard, J. (2019). "Direct and inverse Hopf bifurcation in a neutral delay differential equation model of reed conical instrument," in *Proceedings of the 23rd International Congress on Acoustics*, September 9–13, Aachen, Germany.
- Computational Acoustic Modeling Laboratory (2018). "Analysis and design of saxophone mouthpieces," <http://www.music.mcgill.ca/caml/doku.php?id=projects:adsm> (Last viewed March 12, 2021).
- Coyle, W. L., Guillemain, P., Kergomard, J., and Dalmont, J.-P. (2015). "Predicting playing frequencies for clarinets: A comparison between numerical simulations and simplified analytical formulas," *J. Acoust. Soc. Am.* **138**(5), 2770–2781.
- da Silva, A. R. (2008). "Numerical studies of aeroacoustic aspects of wind instruments," Ph.D. thesis, McGill University, Montreal, Canada.
- Dalmont, J. P. (2007). "Analytical and experimental investigation of the dynamic range of conical reed instruments," in *Proceedings of the International Symposium on Music Acoustics (ISMA) 2007*, September 9–12, Barcelona, Spain.
- Dalmont, J. P., Gazengel, B., Gilbert, J., and Kergomard, J. (1995). "Some aspects of tuning and clean intonation in reed instruments," *Appl. Acoust.* **46**(1), 19–60.
- Dalmont, J.-P., Gilbert, J., and Kergomard, J. (2000). "Reed instruments, from small to large amplitude periodic oscillations and the Helmholtz motion analogy," *Acta Acustica Unit. Acust.* **86**(4), 671–684.
- Dickens, P., Smith, J., and Wolfe, J. (2007). "Improved precision in measurements of acoustic impedance spectra using resonance-free calibration loads and controlled error distribution," *J. Acoust. Soc. Am.* **121**(3), 1471–1481.
- Doc, J.-B., and Vergez, C. (2015). "Oscillation regimes produced by an alto saxophone: Influence of the control parameters and the bore inharmonicity," *J. Acoust. Soc. Am.* **137**(4), 1756–1765.
- Gilbert, J., Maugeais, S., and Vergez, C. (2019). "From the bifurcation diagrams to the ease of playing of reed musical instruments. A theoretical illustration of the Bouasse-Benade prescription?," in *Proceedings of the International Symposium on Music Acoustics (ISMA) 2019*, September 13–17, Detmold, Germany.
- Guillemain, P., Kergomard, J., and Voinier, T. (2005). "Real-time synthesis of clarinet-like instruments using digital impedance models," *J. Acoust. Soc. Am.* **118**(1), 483–494.
- Hirschberg, A., Pelorson, X., and Gilbert, J. (1996). "Aeroacoustics of musical instruments," *Meccanica* **31**(2), 131–141.
- Keefe, D. H. (1990). "Woodwind air column models," *J. Acoust. Soc. Am.* **88**(1), 35–51.
- Kergomard, J., Guillemain, P., Silva, F., and Karkar, S. (2016). "Idealized digital models for conical reed instruments, with focus on the internal pressure waveform," *J. Acoust. Soc. Am.* **139**(2), 927–937.
- Lefebvre, A. (2010). "Computational acoustic methods for the design of woodwind instruments," Ph.D. thesis, McGill University, Montreal, Canada.
- Lefebvre, A., and Scavone, G. P. (2011). "A comparison of saxophone impedances and their playing behaviour," in *Proceedings of 2011 Forum Acusticum*, June 27–July 1, Aalborg, Denmark, pp. 539–544.
- Maestre, E., and Scavone, G. P. (2016). "Experimental modal analysis/synthesis of saxophone input impedances," *J. Acoust. Soc. Am.* **140**(4), 3092–3092.
- Maestre, E., Scavone, G. P., and Smith, J. O. (2018). "Joint modeling of impedance and radiation as a recursive parallel filter structure for efficient synthesis of wind instrument sound," in *Proceedings of the 21st International Conference on Digital Audio Effects*, September 4–8, Aveiro, Portugal, pp. 157–164.
- Maestre, E., Smith, J. O., and Scavone, G. P. (2017). "Analysis-synthesis of saxophone input impedances via recursive parallel filters," in *Proceedings of the 2017 International Symposium on Musical Acoustics (ISMA)*, June 18–22, Montreal, Canada, pp. 105–108.
- Petersen, E., Guillemain, P., Kergomard, J., and Colinot, T. (2019). "The effect of the cutoff frequency on the sound production of a clarinet-like instrument," *J. Acoust. Soc. Am.* **145**(6), 3784–3794.
- Pierce, A. D. (2019). *Acoustics: An Introduction to Its Physical Principles and Applications*, 3rd ed. (Springer, New York).
- Pipes, M. R. (2018). "A comparison of saxophone mouthpieces using Fourier analysis to quantify perceived timbre," Ph.D. dissertation, University of Northern Colorado, Greeley, CO.
- Scavone, G. P. (1997). "An acoustic analysis of single-reed woodwind instruments with an emphasis on design and performance issues and digital waveguide modeling techniques," Ph.D. thesis, Stanford University, Stanford, CA.
- Scavone, G. P. (2002). "Time-domain synthesis of conical bore instrument sounds," in *Proceedings of the 2002 International Computer Music Conference*, September 16–21, Göteborg, Sweden, pp. 9–15.
- Scavone, G. P., and Smith, J. O. (2006). "A stable acoustic impedance model of the clarinet using digital waveguides," in *Proceedings of the 9th International Conference on Digital Audio Effects*, September 18–20, Montreal, Canada, pp. 89–94.
- van Walstijn, M. (2002). Ph.D. thesis, "Discrete-time modelling of brass and reed woodwind instruments with application to musical sound synthesis," University of Edinburgh, Edinburgh, UK.
- van Walstijn, M., and Campbell, M. (2003). "Discrete-time modeling of woodwind instrument bores using wave variables," *J. Acoust. Soc. Am.* **113**(1), 575–585.
- van Walstijn, M., Campbell, M., Kemp, J., and Sharp, D. (2005). "Wideband measurement of the acoustic impedance of tubular objects," *Acta Acust. United Acust.* **91**(3), 590–604.
- van Zon, J., Hirschberg, A., Gilbert, J., and Wijnands, A. P. J. (1990). "Flow through the reed channel of a single reed music instrument," *J. Phys. Colloques* **51**(C2), 821–824.
- Wyman, F. S. (1972). "An acoustical study of alto saxophone mouthpiece chamber design," Ph.D. thesis, Eastman School of Music, University of Rochester, Rochester, NY.